On dynamic models for large eddy simulation

By T. S. Lund

1. Motivation and objectives

1.1 Background

The restriction to low Reynolds numbers is a well known limitation of the direct numerical simulation technique. It is easy to show (*e.g.* Leonard 1973) that the number of grid points required to resolve all the scales of motion increases with the 9/4 power of the Reynolds number. It is clear that direct simulation of high Reynolds flows number found in engineering applications will continue to exceed computer hardware limitations for the foreseeable future.

Fortunately, the inability to simulate all the scales of motion that appear at high Reynolds number can be circumvented by solving a suitably averaged form of the Navier-Stokes equations. The large eddy simulation technique proceeds in this direction by averaging the equations locally over small regions of space. This operation results in a separation of scales into a resolved (large eddy) field and an unresolved (subgrid-scale) field. Much like the familiar Reynolds averaged technique, the large eddy approach leads to a set of governing equations for the resolved field, with the effect of the unresolved scales appearing as an unknown transport term. Unlike the Reynolds averaged technique, this unknown transport term accounts only for the smallest scales of motion. It is generally believed that the smallest scales exhibit a higher degree of isotropy and are more universal in structure that the largest scales of motion. This feature should make the effect of subgrid scales easier to model as opposed to the full range of motions required by the Reynolds averaged approach.

Large eddy simulation in connection with very simple subgrid-scale models has enjoyed a considerable degree of success in modeling high Reynolds number turbulent flows. By far the most popular subgrid-scale model is that of Smagorinsky (1963). This model (as well as a host of variants) is based on a gradient transport hypothesis that leads to an algebraic eddy viscosity formulation. A single model constant is employed, and estimates for its value have been proposed analytically by Lilly (1966), by matching with experimental data (*e.g.* Deardorff 1971, Kwak *et al.* 1975), and by matching with direct simulation data (*e.g.* Clark *et al.* 1979). These various estimates are reasonably consistent for the same type of flow, but considerable variation is evident in dissimilar flows. Bardina *et al.* (1983) showed that the model constant is very sensitive to the level of mean strain rate. The Smagorinsky model apparently does not live up to the ideal of universality; the model constant must be tuned for each type of flow. This drawback limits the utility of large eddy simulation since calibration of the model is a difficult procedure that can be done only if experimental or numerical data exists for the type of flow under consideration.

1.2 Dynamic model of Germano et al.

Recently Germano *et al.* 1991 developed a procedure that overcomes the need to calibrate the Smagorinsky model. In this procedure, information contained in the resolved field is used to determine the value of the Smagorinsky coefficient. This is done, in principal, for each point in the flow at every time step. Aside from removing the tunable constant from the Smagorinsky model, the dynamic procedure has several other advantages: (1) correct behavior is obtained near solid boundaries without the use of *ad hoc* wall damping functions; (2) the subgrid-scale stresses vanish in laminar flow, making transitional calculations possible; and (3) energy transfer from subgrid scales to large scales is possible (*i.e.* backscatter). The dynamic model has been successful in simulating transitional and fully developed channel flow (Germano *et al.* 1991), as well as decaying compressible homogeneous, isotropic turbulence (Moin *et al.* 1991).

Although the dynamic model has demonstrated its advantage over the pure Smagorinsky model, there is one unsettling detail that limits its utility. It turns out that the dynamic procedure yields a model coefficient that has a tremendous variation from point to point in the flow; the rms variation is at least an order of magnitude larger than the spatially averaged mean. Negative values of the model coefficient are just as likely as positive ones, indicating widespread transfer of energy from the subgrid scales to the resolved motions. Isolated occurrences of negative coefficients two to three orders of magnitude greater than the mean have been observed. Large negative coefficients lead to solutions that diverge exponentially, and current numerical methods are not able to handle this behavior. This issue has been circumvented in the aforementioned simulations by averaging the model coefficient over homogeneous directions in the flow. This operation leads to a model coefficient that is almost always positive and of the same order of magnitude as the fixed constants used with the pure Smagorinsky model. As a drawback, the averaging procedure removes the ability of the model to adjust the subgrid-scale stresses to reflect the local behavior of the flow. Furthermore, it is not clear what to do in the case of a flow void of at least one homogeneous direction. Most importantly, the averaging process obscures the issue of whether large negative values of the model coefficient are physically realistic or just an artifact of some inconsistency in the dynamic procedure.

1.3 Objectives

The main objective of this work is to improve the dynamic model of Germano *et al.* so that the local values of the model constant can be used. This objective will be carried out in the following steps:

1. Use direct numerical simulation data to determine to what extent large negative values of the model coefficient are realistic.
2. Determine which elements of the dynamic procedure lead to non-physical model coefficients.
3. Modify the existing model to correct for any exposed defects.
4. Test the modified model against direct numerical simulation data to confirm that the non-physical behavior has been eliminated.

5. Test the modified model in large eddy simulations to evaluate it for accuracy and numerical stability when the local value of the model coefficients are used.

2. Accomplishments

Direct numerical simulation data of turbulent channel flow has been used to isolate problem areas of the dynamic model and to evaluate improvements to the model. The simulation data is that of Kim *et al.* (1987) at Reynolds number of 3300 based on centerline velocity and channel half-width. The grid used in their study contained 128 × 129 × 128 points in the streamwise, normal, and spanwise directions respectively. A synthetic large eddy solution was obtained by interpolating the direct simulation velocity field onto a 64 × 129 × 64 grid using a sharp cutoff filter in Fourier space. The companion subgrid-scale velocity field was formed by subtracting the large eddy field from the direct simulation field. With the subgrid-scale field known, the subgrid-scale stresses could be computed exactly and the results compared with models that operated only on the large eddy component of the velocity field.

Model accuracy was evaluated in terms of the associated dissipation rate. There are two compelling advantages to analyzing the results in this way: (1) dissipation rate is a scalar quantity and thus is easier to interpret than the six components of the subgrid-scale stress tensor; and (2) the most important role of the subgrid-scale model is to dissipate the correct amount of energy from the resolved field. The subgrid-scale dissipation rate is defined as

$$\epsilon = \tau_{mn}\bar{S}_{mn}. \tag{1}$$

Comparisons between exact and modeled dissipation rate were made in terms of scatter plots and in terms of the correlation coefficient, defined as

$$\kappa = \frac{< \epsilon_e \epsilon_m >}{\sqrt{< \epsilon_e^2 >}\sqrt{< \epsilon_m^2 >}}, \tag{2}$$

where ϵ_e and ϵ_m are the exact and model values of the dissipation rate, and $<>$ denotes an average over a plane horizontal to the channel walls. Plane-averaged dissipation rates ($< \epsilon_m >$) were also compared with the corresponding exact values.

2.1 Evaluation of the dynamic model of Germano et al.

Dissipation rates predicted by the dynamic model of Germano *et al.* are compared with exact values in Figures 1-3.

For reference, predictions of a pure Smagorinsky model (identical to that used by Moin and Kim (1982) with ($S_{ij} - < S_{ij} >$) replaced by S_{ij} and $\nu_t^* = 0$) accompany the results of the Germano model. Figure 1 is in the form of a scatter plot where the exact dissipation rate is plotted as function of the modeled dissipation rate. A perfect model would yield a plot where all the points lie on a 45° degree line passing through the origin. Data are displayed for a single horizontal plane, chosen to be the one where the exact dissipation rate is maximized. Figure 1a

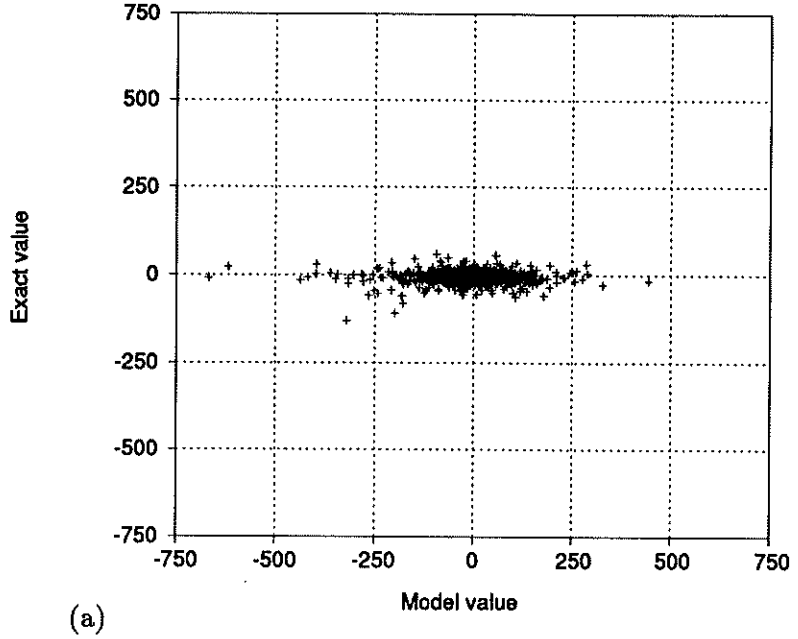

(a)

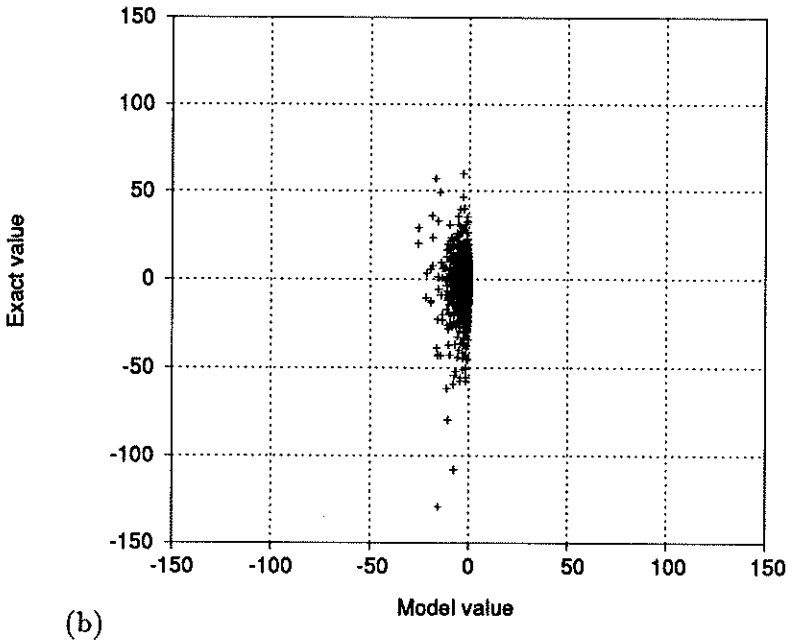

(b)

FIGURE 1. Scatter plots of exact versus modeled dissipation rates for (a) the dynamic model of Germano *et al.* and (b) the Smagorinsky model. Note the difference in scale between plots (a) and (b).

indicates that the dissipation rate predicted by the dynamic model correlates poorly with the exact values. The most striking feature of this plot is that the data lie in a narrow horizontal band, indicating that the model substantially overpredicts the magnitude of the dissipation rate for most points in the flow. The evident symmetry with respect to both the model and exact axes implies that positive dissipation (backscatter) is just as likely as negative dissipation for both the exact and model values. Data for the Smagorinsky model displayed in Figure 1b are remarkably different. The data are aligned in a vertical pattern, indicating that the Smagorinsky model usually underpredicts the magnitude of the dissipation rate. Asymmetry with respect to the model axis is evident, as the Smagorinsky model is constrained to yield only negative dissipation rate. In comparing Figures 1a and 1b, note that the scale in Figure 1a is 5 times larger than that in Figure 1b. This fact, coupled with the different distribution shapes, implies that the dynamic model predicts a span of dissipation rates that is roughly 30 times greater than the Smagorinsky model. More importantly, about half of the dynamic model dissipation rates are positive, indicating energy transfer from the subgrid scales to the large scales. The overprediction of these positive dissipation rates is likely to lead to numerical instability when the dynamic model is installed in a simulation code.

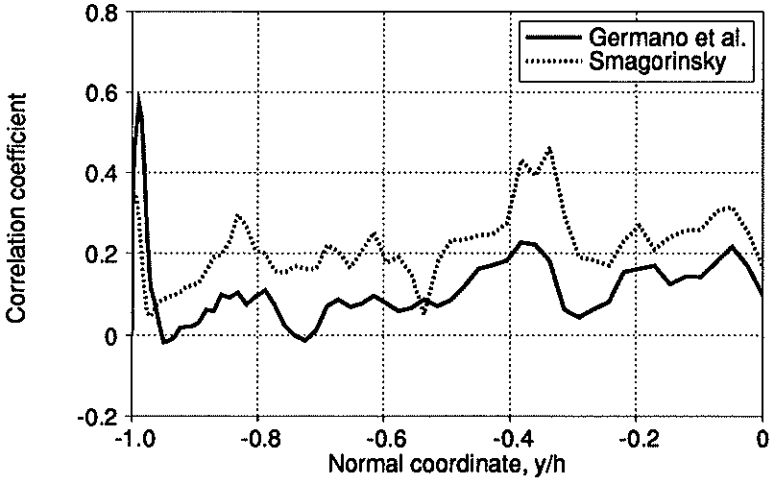

FIGURE 2. Plane averaged correlation coefficient between exact and modeled dissipation rate.

Figure 2 shows the correlation coefficient between the modeled and exact dissipation rate for both the dynamic and Smagorinsky models. The correlations are formed in planes parallel to the channel walls, and the resulting values are plotted as a function of the normal coordinate, with -1 corresponding to the lower channel wall and 0 corresponding to the channel centerline. The correlation is poor for both models except in the near-wall region (where both the modeled and exact subgrid-scale dissipation rate vanish with decreasing distance to the wall). The dynamic

model yields roughly a 10% correlation over most of the channel, which is about half the roughly 20% produced by the Smagorinsky model. The correlation coefficient for the dynamic model is seen to be negative at a few locations, which indicates that the model predicts dissipation of the wrong sign for a significant number of points within these planes.

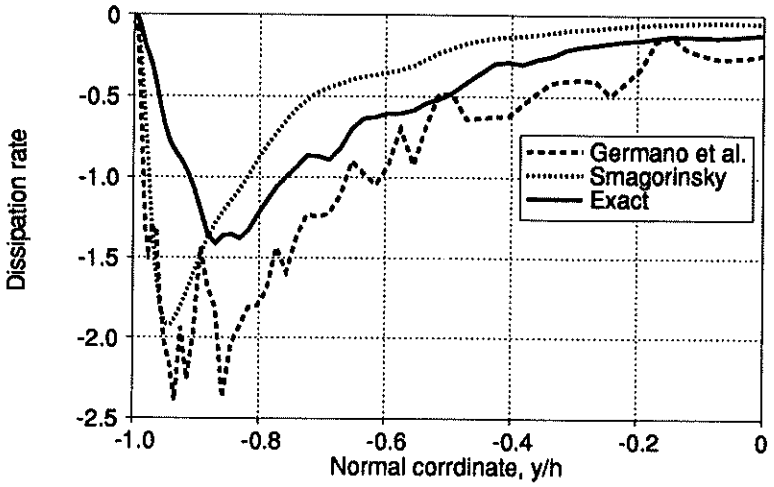

FIGURE 3. Plane averaged dissipation rate.

Dissipation rates averaged over planes parallel to the channel walls are displayed in Figure 3. It is evident that both the dynamic and Smagorinsky models are in fair agreement with the exact values. The dynamic model is much noisier, probably as a result of the wider range of values within each plane. In view of the results shown in the scatter plots of Figure 1, it is remarkable that both models yield reasonable average values of dissipation rate. In the case of the dynamic model, the abundance of both large positive and negative values evidently cancel, leaving a small negative residual. In the case of the Smagorinsky model, the distribution is very tightly packed about a small negative value. Since the model constant was properly tuned by Moin and Kim, the distribution is also centered about the correct value. Notice when comparing Figures 1 and 3 that the average value of dissipation rate is of order 1, while the range of exact values is of order 100, and the range predicted by the dynamic model is of order 1000.

2.2 Comments on the dynamic model of Germano et al.

It has been shown that the dynamic model locally overpredicts magnitude of the dissipation rate and is very weakly correlated with the exact values. At the same time, however, the model predicts the average dissipation rate with acceptable accuracy. These results are consistent with the calculations of Germano *et al.* (1991) and Moin *et al* (1991) where accurate results were obtained using averaged values of

the model and where numerical instabilities prevented performing calculations using local values of the model coefficient. It is hypothesized here that the numerical difficulties experienced in the aforementioned investigations was due to both local areas of non-physically large values of positive dissipation and prediction of positive dissipation rate when it should be negative. Positive dissipation rates lead to exponential growth in the velocity field, and the solution will increase without bound until the dissipation rate reverses sign. The propensity of the Germano model to overpredict the values of positive dissipation rate, coupled with its tendency to predict erroneous positive dissipation rates, makes it seem likely that rapidly growing solutions could be incorrectly amplified rather than damped. If this scenario is correct, then it is the noisy nature of the dynamic model that is responsible for the numerical difficulties. The model is scrutinized for the source of its noise in the following subsection

2.2.1 Stress-strain alignment and local isotropy

The dynamic model is constructed from the following chain of equalities

$$\underbrace{(\widehat{\bar{u}_i\bar{u}_j} - \hat{\bar{u}}_i\hat{\bar{u}}_j) - \frac{1}{3}(\widehat{\bar{u}_k\bar{u}_k} - \hat{\bar{u}}_k\hat{\bar{u}}_k)\delta_{ij}}_{\text{computable}} = \underbrace{L^*_{ij} \equiv T^*_{ij} - \hat{\tau}^*_{ij}}_{\text{Germano's identity}}$$

$$= -C\bar{\Delta}^2 \underbrace{\left[\left(\frac{\hat{\Delta}}{\bar{\Delta}}\right)^2 |\hat{\bar{S}}|\hat{\bar{S}}_{ij} - \widehat{|\bar{S}|\bar{S}_{ij}}\right]}_{M_{ij}\ \text{(computable)}}, \quad (3)$$

where $\bar{()}$ denotes variables obtained directly from the large eddy simulation, $\hat{()}$ denotes a "test" filtering operation that removes the smallest scales resolved by the large eddy simulation, and $*$ denotes the trace-free part of the corresponding tensor. C is the square of the usual Smagorinsky coefficient, S_{ij} is the strain rate, Δ is a measure of the grid spacing, and T and τ are the subgrid-scale stresses associated with the test-filtered and large eddy fields, respectively. Notice that the Smagorinsky model has been assumed for both stress fields, with the same value of the scaling coefficient (which, when defined locally, has been inconsistently extracted from the test filtering operation in the last term).

Equation (3) may be written more compactly as

$$L^*_{ij} = -C\bar{\Delta}^2 M_{ij}. \quad (4)$$

Since both L^* and M are computable, the above relation can, in principal, be solved to yield the value of C. Notice, however, that the above equation is a tensor relation that is equivalent to nine scalar equations (only six of which are independent due to symmetry). Two possibilities thus exist: either (1) L^* and M are the same tensor, differing only by a scaling factor, or (2) the system is overdetermined algebraically and no value of C will make Eq. (4) an equality. The former requirement is met

if the Smagorinsky models used at both the large eddy and test-filtered levels are exactly correct. In this case, the subgrid-scale stress and the corresponding strain rate tensors are related by a scalar factor and therefore share the same principal directions (perfect alignment). Alignment of the subgrid-scale stresses and the strain rate implies that the subgrid-scale stresses are transporting momentum isotropically at each point within the flow field. Isotropy, however, is a statistical notion that is not expected to hold locally. Indeed, the scatter plot of Figure 1(b) confirms this conjecture by illustrating the poor correlation between the Smagorinsky model and the exact values on a point-to-point basis.

It can be argued that while the Smagorinsky model is not strictly valid from point to point, it is still a reasonable approximation. Using this line of reasoning, each of the six constraints implied by Eq. (4) would yield a different value of C, but the variation between these values would be small. It is easy to show that this variation can be minimized in a least squares sense by simply contracting both sides of Eq. (4) with the model terms M_{ij}. The resulting scalar equation can then be solved to obtain a unique value of C.

The degree of success achieved by the least squares approach can be evaluated through the use of the following correlation coefficient that is the tensorial analog of the cosine of the angle between two vectors

$$\kappa = \frac{M_{mn} L^*_{mn}}{\sqrt{M^2}\sqrt{L^{*2}}} \tag{5}$$

where $M^2 = M_{mn} M_{mn}$. If the correlation coefficient is unity, the tensors M and L^* are perfectly aligned and the six constraints implied by Eq. (4) are identical. Values of the correlation coefficient slightly less than unity imply reasonable alignment between L^* and M, corresponding to a small degree of incompatibility among the constraints of Eq. (4). A correlation coefficient near zero indicates that L^* and M are nearly orthogonal and the constraints of Eq. (4) are strongly incompatible. Negative values of the correlation coefficient have the same relative meaning, but with the principal directions of L^* and M having the opposite sense.

The correlation coefficient between L^* and M, averaged over planes parallel to the channel walls is displayed in Figure 4. In forming the average, the absolute value of the correlation coefficient has been taken to avoid a fortuitous cancellation between positive and negative values (negative values imply local backscatter). Also included in Figure 4 are the correlation coefficients between T^* and $\hat{\bar{S}}$ and τ^* and $\bar{S}$. All three correlations are quite similar. The correlations are nearly zero close to the wall, from where they rise to a roughly constant value of 0.35 for most of the channel. The extremely poor correlation near the wall is not surprising since anisotropy is greatest in this region.

The low degree of correlation between T^* and $\hat{\bar{S}}$, and τ^* and $\bar{S}$ invalidates the assumed isotropic relationship between subgrid-scale stress and strain rate incorporated in the Smagorinsky model. When the dynamic procedure is applied to the Smagorinsky model, the resulting equations for the coefficient C (Eq. (4)) attempt

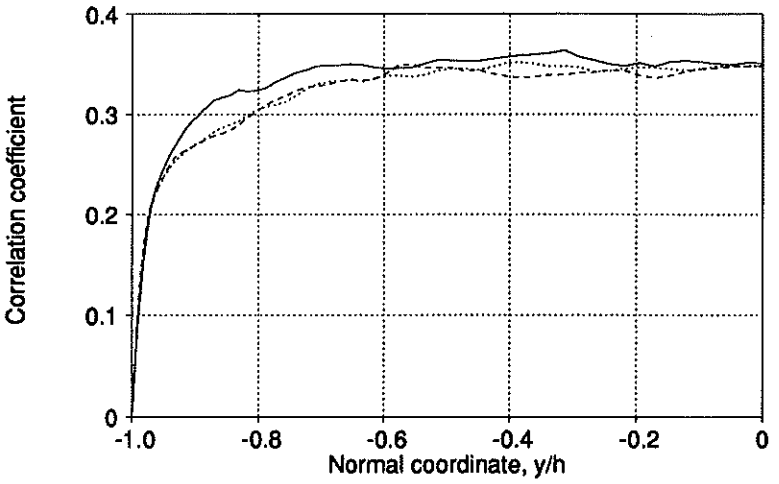

FIGURE 4. Plane averaged tensor correlation coefficients. ——— , L^*M; ---- , $\tau^*\bar{S}$; ····· , $T^*\hat{\bar{S}}$.

to force this isotropic relation to hold. The resulting equations are inherently inconsistent, and as evidenced by the low correlation between L^* and M, the least squares approach can be expected to yield erroneous results.

2.3 A principal alignment dynamic model

In light of the conclusions drawn in the previous section, it is clear that an isotropic subgrid-scale stress model such as that of Smagorinsky leads to a poorly conditioned set of equations for the model coefficient. The difficulty stems from the assumed alignment between the subgrid-scale stress and the strain rate. The assumed alignment carries through to Eq. (4), where an inconsistency arises since the computed tensors L^* and M are not aligned. This difficulty can be alleviated through use of a model that does not assume alignment but rather performs operations on $\bar{S}$ to align it with τ. Such an anisotropic model is developed in this section.

In developing the new model, it is most convenient to think in terms of principal coordinates. Since both the subgrid-scale stress and the strain rate are real symmetric tensors, each may be decomposed into three principal values and a corresponding set of three mutually orthogonal principal directions. Thinking in these terms, the strain rate tensor can be transformed exactly into the subgrid-scale tensor as follows. First, each of the three principal values of $\bar{S}$ is independently stretched to match the corresponding principal value of τ. Next, the principal directions of $\bar{S}$ are subjected to three independent rotations to line them up with the principal directions of τ. Note that 6 degrees of freedom (three stretchings and three rotations) are needed to match the principal values and align the principal directions of $\bar{S}$ and τ. This is precisely the number of constraints that will arise from the dynamic procedure (*cf.* Eq. (4)). Thus if the principal alignment procedure is followed, there will be a

uniquely determined solution for the stretchings and rotations.

The principal alignment procedure is now developed. Using matrix notation, τ and $\bar{S}$ are decomposed as follows

$$\tau = X_\tau \Lambda_\tau X_\tau^{-1}, \qquad \bar{S} = X_{\bar{s}} \Lambda_{\bar{s}} X_{\bar{s}}^{-1}, \tag{6a,b}$$

where X_τ, X_τ^{-1}, and $X_{\bar{s}}$, $X_{\bar{s}}^{-1}$ are the normalized eigenvector matrix and inverse for τ and $\bar{S}$, respectively, while Λ_τ and $\Lambda_{\bar{s}}$ are diagonal matrices of the corresponding eigenvalues. The eigenvectors yield the principal directions, while the eigenvalues give the principal values. Starting with Eq. (6a) and using Eq. (6b) it is possible to write the following

$$\begin{aligned} \tau &= X_\tau \Lambda_\tau X_\tau^{-1} \\ &= X_\tau \left(\frac{\Lambda_\tau}{\Lambda_{\bar{s}}} \right) \Lambda_{\bar{s}} X_\tau^{-1} \qquad (7a) \\ &= X_\tau \left(\frac{\Lambda_\tau}{\Lambda_{\bar{s}}} \right) X_{\bar{s}}^{-1} \bar{S} X_{\bar{s}} X_\tau^{-1}, \qquad (7b) \end{aligned}$$

where the ratio $\Lambda_\tau / \Lambda_{\bar{s}}$ is equivalent to $\Lambda_{\tau_k} / \Lambda_{\bar{s}_k}$ in index notation. The eigenvalue ratios perform the required stretchings while the eigenvector products perform the required rotations. Equation (7b) has been included for clarity only; Eq. (7a) is the desired form. Note that Eq. (7a) requires the principal values and principal directions of τ. These can be estimated from the corresponding eigensystem of T.

If it is assumed that τ scales with $\bar{\Delta}^2 |\bar{S}|^2$, and T with $\hat{\Delta}^2 |\hat{\bar{S}}|^2$, then the following relation will hold

$$\frac{\Lambda_\tau}{\Lambda_{\bar{s}}} = \left(\frac{\bar{\Delta}}{\hat{\Delta}} \right)^2 \frac{|\bar{S}|}{|\hat{\bar{S}}|} \frac{\Lambda_T}{\Lambda_{\hat{s}}}. \tag{8}$$

If it is assumed further that τ and T share the same principal directions, then Eqs. (7a) and (8) can be combined to give

$$\tau = X_T \left[\left(\frac{\bar{\Delta}}{\hat{\Delta}} \right)^2 \frac{|\bar{S}|}{|\hat{\bar{S}}|} \left(\frac{\Lambda_{\bar{s}}}{\Lambda_{\hat{s}}} \right) \Lambda_T \right] X_T^{-1}. \tag{9}$$

Thus τ may be expressed in terms of the eigensystem of T. The eigensystem of T is determined from Germano's identity (Eq. (3)) as follows

$$L_{ij} = T_{ij} - \hat{\tau}_{ij} \simeq T_{ij}. \tag{10}$$

This approximation is justified on the grounds that the dominant contribution to τ are the precisely the highest frequencies that are removed by the filtering operation done in forming $\hat{\tau}$. As illustrated in Figure 5, this approximation becomes increasingly better as the filter width ratio $\hat{\Delta}/\bar{\Delta}$ is increased.

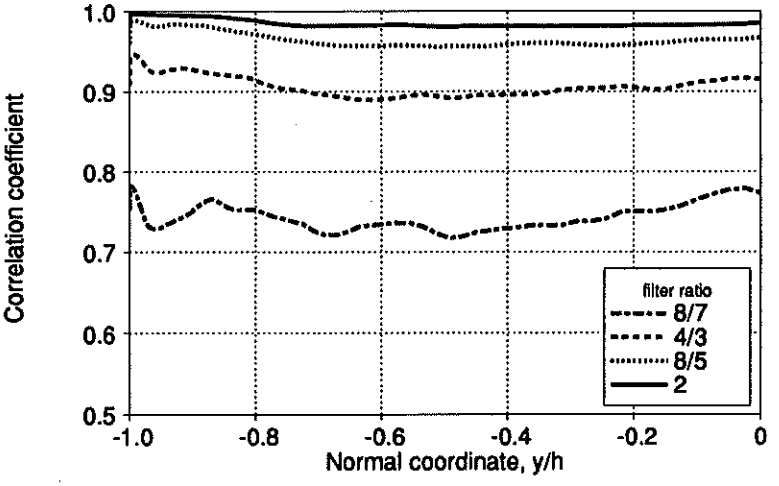

FIGURE 5. Plane averaged correlation coefficient between the tensors T and L as a function of filter width ratio.

With the eigensystem of T approximated by the eigensystem of L, Eq. (9) takes the final form

$$\tau = X_L \left[\left(\frac{\bar{\Delta}}{\hat{\Delta}} \right)^2 \frac{|\bar{S}|}{|\hat{\bar{S}}|} \left(\frac{\Lambda_{\bar{s}}}{\Lambda_{\hat{\bar{s}}}} \right) \Lambda_L \right] X_L^{-1}. \tag{11}$$

2.4 Tests of the principal alignment model

The model developed in the previous section is subjected to the same tests given to the dynamic model of Germano *et al.* in Section 2.1.

A scatter plot of the subgrid-scale dissipation is shown in Figure 6. The correlation between model and exact values is seen to be fair. Even though the correlation is only fair, it is a marked improvement from that corresponding to the dynamic model. Note that the range of dissipation predicted by the principal alignment model is roughly a factor of 10 less than that for the dynamic model. This is significant since erroneously large values of positive dissipation are likely to lead to numerical instability. The principal alignment model is also superior to the Smagorinsky model in the sense that it is able to predict backscatter. Plane averages of the correlation coefficient between the model and exact values of dissipation rate are shown in Figure 7.

The principal alignment model is seen to correlate somewhat better with the exact values than does the dynamic model. There is still a local region of negative correlation. This is an unsettling detail that will be addressed in future improvements to the model. Plane averaged dissipation rate is shown in Figure 8. Agreement with the exact values is seen to be good.

3. Summary and future plans

The primary motivation for this work was to eliminate the numerical difficulties

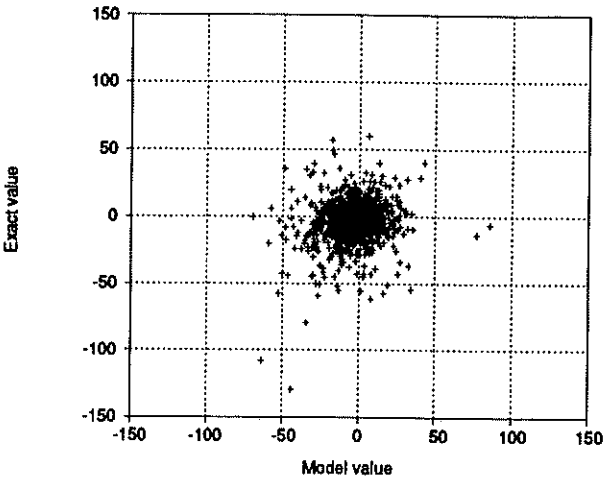

FIGURE 6. Scatter plot of exact versus modeled value of dissipation rate for the principal alignment model.

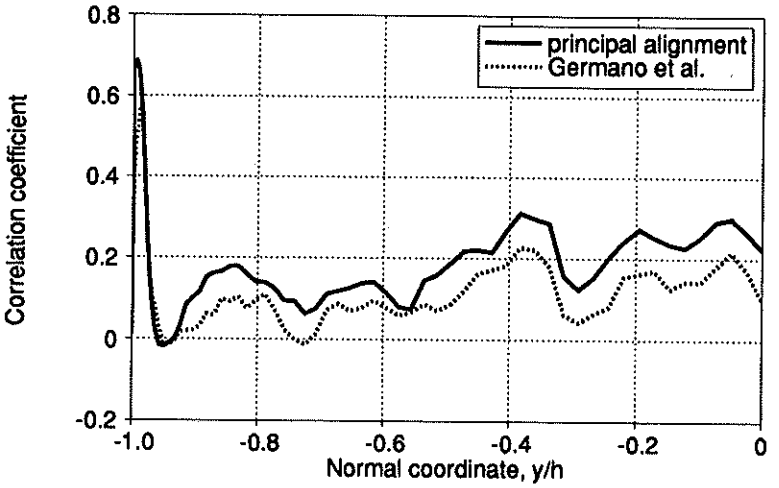

FIGURE 7. Plane averaged correlation coefficient between exact and modeled dissipation rate for the principal alignment model.

associated with the model of Germano *et al.* when local values of the model constant are used. It was shown that the subgrid-scale stresses are not related isotropically to the strain rate on a point to point basis. The Smagorinsky model is, therefore, not valid in this sense, and its use in the dynamic procedure leads to an inconsistent set of equations for the model coefficient. It was further shown that a more general, non-isotropic relation between the subgrid-scale stresses and the strain rate leads to

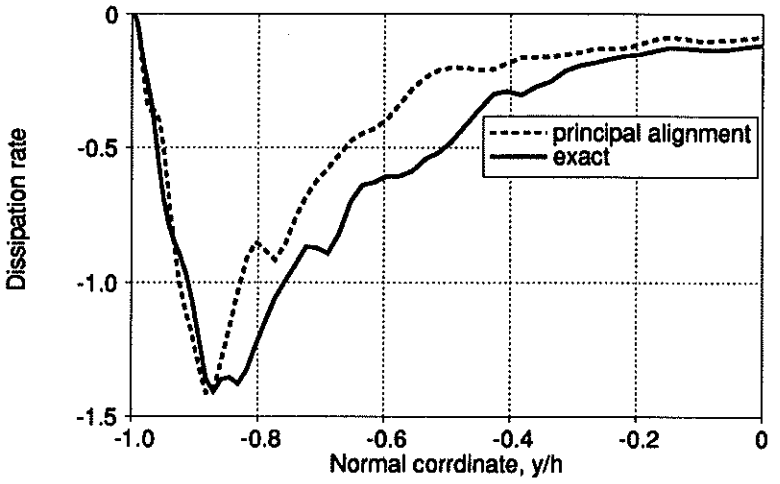

FIGURE 8. Plane averaged dissipation rate.

a dynamic model that correlates better with the exact values and contains roughly an order of magnitude less erroneous scatter.

The next step in this work will be to test the principal alignment model in a large eddy simulation to evaluate it for numerical stability and accuracy. This will be done initially in simulations of isotropic, homogeneous turbulence. This phase is currently being implemented, and preliminary indications are that the principal alignment model does not lead to instability. The accuracy of the model is yet unchecked. If simulations in homogeneous turbulence are successful, the new model will be applied to the more challenging case of turbulent channel flow.

Improvements to the model will also be made. The principal alignment model still has a tendency to predicts dissipation of the wrong sign (points in quadrants 2 and 4 in Figure 6). Modifications will be sought to reduce this effect.

REFERENCES

BARDINA, J., FERZIGER, J. H. & REYNOLDS, W. C. 1983 Improved turbulence models based on large eddy simulation of homogeneous, incompressible, turbulent flows. *Report No. TF-19,* Thermosciences Div., Dept. of Mech. Engrg., Stanford University, Stanford CA.

CLARK, R. A., FERZIGER, J. H., & REYNOLDS, W. C. 1979 Evaluation of subgrid-scale models using an accurately simulated turbulent flow. *J. Fluid Mech.* **91,** 1-16.

DEARDORFF, J. W. 1971 On the magnitude of the subgrid-scale eddy coefficient. *J. Comp. Phys.* **7,** 120-133.

GERMANO, M., PIOMELLI, U., MOIN, P., & CABOT, W. H. 1991 A dynamic subgrid-scale eddy viscosity model. *Phys. Fluids A.* **3,** 1760-1765.

KIM, J., MOIN, P., & MOSER, R. 1987 Turbulent statistics in fully developed channel flow at low Reynolds number. *J. Fluid Mech.* **177**, 133-166.

KWAK, D., REYNOLDS, W. C., & FERZIGER, J. H. 1981 Three-dimensional time-dependent computation of turbulent flows turbulent fluid flows . *Report No. TF-5,* Thermosciences Div., Dept. of Mech. Engrg., Stanford University, Stanford CA.

LEONARD, A. 1973 Energy cascade in large-eddy simulations of turbulent fluid flows. *Adv. Geophys.* **18A**, 237-248.

LILLY, D. K. 1966 On the application of the eddy viscosity concept in the inertial sub-range of turbulence. *NCAR manuscript 123,* National Center for Atmospheric Research, Boulder CO.

MOIN, P., & KIM, J. 1982 Numerical investigation of turbulent channel flow . *J. Fluid Mech.* **118**, 341-377.

MOIN, P. SQUIRES, K., CABOT, W., & LEE, S. 1991 A dynamic subgrid-scale model for compressible turbulence and scalar transport. *Phys. Fluids A* . **3**, 2746-2757.

SMAGORINSKY, J. 1963 General circulation experiments with the primitive equations. *Mon. Weather Rev.* **91**, 99-164.